

Engineering interaction potentials for stabilizing quantum quasicrystal phases

Matheus Grossklags,^{1,*} Daniel Lima,¹ Vinicius Zampronio,^{2,†} Fabio Cinti,^{2,3,4,‡} and Alejandro Mendoza-Coto^{1,2,§}

¹*Departamento de Física, Universidade Federal de Santa Catarina, 88040-900 Florianópolis, Brazil*

²*Dipartimento di Fisica e Astronomia, Università di Firenze, I-50019, Sesto Fiorentino (FI), Italy*

³*INFN, Sezione di Firenze, I-50019, Sesto Fiorentino (FI), Italy*

⁴*Department of Physics, University of Johannesburg,
P.O. Box 524, Auckland Park 2006, South Africa*

We investigate the necessary features of the pair interaction for the stabilization of self-assembled quantum quasicrystals in two-dimensional bosonic systems. Unlike the classical scenario, our results show that two-dimensional octagonal, decagonal, and dodecagonal aperiodic phases require a distinct number of properly tuned characteristic length scales for their stabilization. By using a mean field spectral variational approach and Gross-Pitaevskii numerical calculations, we determine that the dodecagonal quasicrystal structure requires at least two characteristic length scales for its stabilization, while the decagonal and octagonal patterns need at least three and four length scales, respectively. The family of pair interaction potentials considered, albeit simple, is well justified in terms of a novel experimental platform based on laser-painted interactions in a cavity QED setup. Finally, we perform a structural characterization of the quasicrystal patterns obtained and show that these phases coexist with a finite superfluid fraction, forming what can be called a super quasicrystal phase.

I. INTRODUCTION

The self-assembly of complex phases such as cluster crystals¹⁻⁴, quasicrystals⁵⁻¹⁴, supersolids¹⁵⁻²⁰, and topological phases²¹⁻²⁷ is a central topic of many-body physics, with applications in soft matter²⁸⁻³² and hard condensed matter³³⁻⁴⁰. In particular, quasicrystals in two and three dimensions are characterized by a lack of spatial periodicity while exhibiting long-range n -fold rotational symmetry (with $n > 6$) forbidden by conventional crystallography⁴¹⁻⁴³. In classical systems of particles, the formation of cluster quasicrystals typically arise in the presence of isotropic soft-core pair potentials with competing length scales^{10,11}, like in the case of dendritic macromolecules^{44,45}. The existence of two degenerate minima in the Fourier transform of the interaction at the appropriate wave vectors controls the self-assembly process of quasicrystals¹⁰. In this scenario, the specific values chosen for the ratio between characteristic length scales in the system determines the rotational symmetry of the structure to be stabilized. Such interplay between length scales has been extensively studied in the Lifshitz-Petrich-Gaussian model^{10,46} due to its mathematical flexibility, which allows the stabilization of periodic and aperiodic phases as the minima structure of the potential and thermal fluctuations are tuned.

These insights have recently guided the search for novel quantum phases, showing that the combined effect of tailored interactions and quantum fluctuations can similarly stabilize quantum quasicrystals^{12-14,47}. Interestingly, all studies focusing on quantum self-assembled quasicrystals

analogous to the one considered by Barkan et al.¹⁰, but at zero temperature, have been related to the stabilization of a dodecagonal phase. In this case, the literature^{13,48} seems to indicate that to enhance stability or even to achieve the stabilization of these phases at all, either the higher momentum minimum should be deeper than the low momentum minimum, or extra resonant incommensurate minima should be added to the pair interaction potential. In this scenario, to push forward the comprehension of the necessary properties of the pair interaction potential for the stabilization of quantum quasicrystals, it is essential to consider scenarios with different rotational symmetries.

Ultracold atoms provide a versatile platform for investigating quantum quasicrystals. With precise control over both internal and external degrees of freedom, these systems have been used to simulate a wide range of quantum phases⁴⁹⁻⁵⁴. However, the realization of quasicrystals^{52,55} and other exotic phases^{56,57} often requires long-range or oscillatory interactions, which are not typically accessible in systems of quantum gases. One novel approach involves the use of a high-finesse optical cavity and a beam shaped laser scanning the system to produce tailored effective sign-changing interactions between the atoms of the system⁵⁸. In this work, the authors show that the effective interaction having the form $\hat{V}(\mathbf{q}) = g_{aa} - \Delta \hat{\Omega}(\mathbf{q})^2$, is controlled by the Fourier transform of the Rabi frequency profile of the laser $\hat{\Omega}(\mathbf{q})$, the original contact interaction between atoms g_{aa} and the parameter Δ accounting for microscopic details of the quantum mechanism involved in the interaction process. The resulting expression offers an unprecedented degree of customization, providing the same level of flexibility of the Lifshitz-Petrich-Gaussian model for the production of classical quasicrystals and other modulated phases. Although this pioneering protocol has not been tested experimentally yet, similar setups have been successfully

* matheus.grossklags@posgrad.ufsc.br

† v.zampronio@unifi.it

‡ fabio.cinti@unifi.it

§ alejandro.mendoza@ufsc.br

used already to stabilize supersolids^{59,60}, spin textured phases^{52,56,61}, and extended Hubbard models^{62,63}.

In the present paper, we use a mean field spectral variational approach^{13,14,64} to explore the engineering principles of the pair interaction potential in Fourier space for the stabilization of three prominent quantum quasicrystal phases with octagonal, decagonal, and dodecagonal rotational symmetries. We systematically consider the effects of having two or more competing length scales in the pair potential properly tuned in order to stabilize the corresponding quasicrystal phase and enhance its extension in the ground state phase diagram. We show that, in contrast to the classical scenario, the stabilization of quantum quasicrystals with different rotational symmetries requires pair interaction potentials with a very distinct minima structure. Next, we investigate the reasons for the much greater stability of the dodecagonal structure in comparison to the decagonal and octagonal patterns and present a geometric argument clarifying the origin of such phenomenon. Moreover, to deepen our understanding on the reported phases, we analyze the behavior of the superfluid fraction in three particular cases showing that quasicrystalline order can coexist with global superfluidity, exhibiting a phase analogous to the supersolid phase. We employed two contrasting methods to study the superfluidity, the mean field spectral variational method and the numerical solution of the real-space Gross-Pitaevskii equation in imaginary time, showing that both techniques provide equivalent results. Finally, we discuss the results and present the concluding remarks of our work.

The paper is organized as follows: In Section II we introduce the model Hamiltonian and the applied methodology, while Section III presents results concerning the dodecagonal structure. Decagonal quasicrystal is presented in Section IV. Finally in Section V we discuss the octagonal setup. Section VI is devoted to our final remarks and conclusions.

II. MODEL AND METHOD

We consider a two-dimensional gas of N bosonic particles with mass m at zero temperature interacting with a pair potential $V(\mathbf{x})$. Within the mean field approximation, valid at high density of particles and weak enough interactions, the total energy of the system can be expressed as

$$E[\phi] = \frac{\hbar^2}{2m} \int d^2x |\nabla\phi(\mathbf{x})|^2 + \frac{1}{2} \int d^2x d^2x' V(\mathbf{x} - \mathbf{x}') \times |\phi(\mathbf{x})|^2 |\phi(\mathbf{x}')|^2, \quad (1)$$

where $\phi(\mathbf{x})$ stands for the wave function of the condensate, satisfying the normalization condition $\int d^2x |\phi(\mathbf{x})|^2 = N$. Moreover, we consider that the pair interaction potential is written in momentum space as

$\hat{V}(\mathbf{q}) = g_{\text{aa}} - \Delta \hat{\Omega}(\mathbf{q})^2$, such model of pair interaction was presented and discussed earlier in the introduction section. For a study of the stabilization conditions of distinct quasicrystal structures, we consider a rather simple laser beam model in momentum space $\hat{\Omega}(\mathbf{q})$, given by the superposition of several Gaussian profiles centered at different momenta with negligible overlapping between them. As a consequence, the pair interaction potential $\hat{V}(\mathbf{q})$ exhibits a series of local minima properly positioned in order to favor the stabilization of a particular quasicrystalline pattern^{13,14}.

To stabilize a quasicrystal exhibiting n -fold rotational symmetry with characteristic momentum q_1 , it is expected that in addition to q_1 , other resonant momenta associated with the corresponding quasicrystal structure should also be excited. In general, if we combine two wave vectors of the extended basis $\mathbf{q}_i = q_1 (\cos(2\pi i/n), \sin(2\pi i/n))$ with $i = 0, 1, \dots, n-1$, we obtain the first group of secondary characteristic wave vectors of the corresponding pattern. For the three simplest and most relevant quasicrystalline structures, octagonal, decagonal, and dodecagonal, $n = 8, 10$, and 12 , respectively, the first group of secondary wave vectors contains three or more different sets of vectors with an incommensurate length with respect to the characteristic wave vector. Taking this into account, our approach to study the stabilization of quasicrystalline patterns involves separately exciting these length scales in $\hat{\Omega}(\mathbf{q})$, thus clarifying the necessary number of minima in $\hat{V}(\mathbf{q})$ for the desired quasicrystal stabilization. In this way, we consider

$$\hat{\Omega}(\mathbf{q}) = \sum_{j=1}^4 \omega_j \exp\left(-\frac{(q - q_j)^2}{\alpha_j^2}\right), \quad (2)$$

where ω_j , α_j and q_j are positive parameters measuring the intensity, width and characteristic momentum of each Gaussian peak in $\hat{\Omega}(\mathbf{q})$, respectively. As previously discussed, once the characteristic momentum is set by the main peak in $\hat{V}(\mathbf{q})$, the position of the secondary modes to be excited are located at specific irrational numbers in units of q_1 .

Considering q_1 the main wave vector of the quasicrystal structure as our unit of momentum, it is natural to choose $\lambda = 1/q_1$ and $\epsilon = \hbar^2/m\lambda^2$ as units of length and energy, respectively. Hence, the dimensionless vector position and momentum are defined as $\mathbf{r} = \mathbf{x}/\lambda$ and $\mathbf{k} = \mathbf{q}/q_1$. Considering these units of energy and length, the dimensionless energy per particle functional for our model writes

$$\frac{E[\psi]}{N\epsilon_0} = \frac{1}{2} \int \frac{d^2r}{A} |\nabla\psi(\mathbf{r})|^2 + \frac{\lambda^2 U \rho}{2} \int \frac{d^2r d^2r'}{A} v(\mathbf{r} - \mathbf{r}') |\psi(\mathbf{r})|^2 |\psi(\mathbf{r}')|^2, \quad (3)$$

where A stands for the area of the system and $\psi(\mathbf{r})$ represents the normalized wave function, satisfying $\int_A d^2r |\psi(\mathbf{r})|^2 = A$. Furthermore, the effective pair interaction potential $Uv(\mathbf{r})$ corresponds originally to $V(\mathbf{x})/\epsilon$.

Here, we have introduced the dimensionless parameter U to quantify the intensity of the pair interaction potential and $v(\mathbf{r})$ to encode the information about its spatial variation. To avoid any ambiguity in this definition we impose additionally that $\hat{v}(k=1) = -1$, without generality loss. Under these conditions, the local dimensionless density of particles is given by $\rho(\mathbf{r}) = \lambda^2 \rho |\psi(\mathbf{r})|^2$, where ρ represents the average particles density. It is worth noticing that within our framework the dimensionless parameter $\lambda^2 U \rho$ controls the relative intensity of the potential energy contribution in comparison to the kinetic energy in the ground-state energy functional, or in other words the intensity of the quantum fluctuations (zero point motion) in our system. In this way, $\lambda^2 U \rho$ is naturally one of the running parameter of the phase diagrams for the models considered.

To proceed, we consider that the ground-state wave function $\psi(\mathbf{r})$ minimizing the energy-per-particle functional can be written in a Fourier basis. In this way, we propose^{13,16}

$$\psi(\mathbf{r}) = \frac{1 + \frac{1}{2} \sum_{j \neq 0} c(\mathbf{k}_j) \cos(\mathbf{k}_j \cdot \mathbf{r})}{\left(1 + \frac{1}{4} \sum_{j \neq 0} c(\mathbf{k}_j)^2\right)^{1/2}}, \quad (4)$$

where $c(\mathbf{k}_j)$ and \mathbf{k}_j represent the Fourier amplitudes and wave vectors of the expansion. The set of wave vectors and amplitudes $\{\mathbf{k}_j, c(\mathbf{k}_j)\}$ defines the type of modulated pattern under consideration and its symmetries. These wave vectors are constructed as all possible integers combinations of a vector basis $\{\mathbf{k}_{j,0}\}$, the number of elements of the basis defines the rank of the solution. In two dimensions, periodic pattern solutions correspond to configurations of rank 2 or smaller, while quasicrystals have a rank higher than 2. In Table I, we present the list of solutions considered as well as its wave vector basis, here the variational parameter k_m sets the scale of the wave vectors lattice. In terms of possible solutions, we consider all periodic patterns typically found in quasicrystal forming systems¹⁰: one dimensional modulations, i.e., stripes, 2D hexagonal and square crystalline patterns, as well as two different kinds of compressed hexagonal patterns exciting simultaneously the two dominant characteristic wave vectors of the pair potential^{65–67} and finally, n -fold rotationally symmetric quasicrystals with $n = \{8, 10, 12\}$. Within the mean field spectral variational analysis, the set of Fourier amplitudes $\{c_j\}$ and the characteristic momentum k_m for each possible solution are determined from the minimization of the corresponding energy-per-particle functional^{29,68}. Finally, the ground state is calculated selecting the solution with the lowest energy. For the special case of the homogeneous solution, all coefficients c_j vanish except for $c_0 = 1$. It is important to observe that the variational complexity of our problem can be significantly reduced by recognizing that Fourier amplitudes c_j 's corresponding to equivalent wave vectors \mathbf{k}_j 's after symmetry operations of the associated density pattern should be equal. For numerical purposes, the Fourier expansion in Eq. (4) for each kind of solu-

Pattern	Vector basis $\mathbf{k}_{j,0}$	Index range
Stripes	$k_m (1, 0)$	
Square	$k_m (\cos(2\pi j/4), \sin(2\pi j/4))$	$j = 0, 1$.
Hexagonal	$k_m (\cos(2\pi j/6), \sin(2\pi j/6))$	$j = 0, 1$.
Comp. Hex.1	$k_m \left(1/2, \pm \sqrt{\tilde{k}_2^2 - 1/4}\right)$	
Comp. Hex.2	$k_m \left(\tilde{k}_2/2, \pm \sqrt{1 - \tilde{k}_2^2/4}\right)$,	
8-QC	$k_m (\cos(2\pi j/8), \sin(2\pi j/8))$	$j = 0, \dots, 3$.
10-QC	$k_m (\cos(2\pi j/10), \sin(2\pi j/10))$	$j = 0, \dots, 3$.
12-QC	$k_m (\cos(2\pi j/12), \sin(2\pi j/12))$	$j = 0, \dots, 3$.

Table I. Modulated patterns considered in this work and their corresponding wave vector basis $\mathbf{k}_{j,0}$. The list of possible solutions includes: stripes, square and hexagonal crystalline patterns, compressed hexagonal patterns exciting simultaneously wave vectors on the ratio \tilde{k}_2 (see Table II) and quasicrystalline patterns with eight- (8-QC), ten- (10-QC) or twelve-fold (12-QC) rotational symmetry.

tion is truncated using a large enough set of modes to guarantee energy convergence. Moreover, the truncation process employed guarantees that the symmetries of the corresponding pattern are fully preserved by the truncated ansatz solution.

A. Pair interaction potential

Considering the model proposed for the laser profile $\hat{\Omega}(\mathbf{q})$, we represent the dimensionless pair interaction potential $\hat{v}(k)$ in the general form

$$\hat{v}(k) = g - \left(\sum_{j=1}^4 d_j \exp \left[- \left(k - \tilde{k}_j \right)^2 / \sigma_j^2 \right] \right)^2, \quad (5)$$

As a consequence of our choice of length and energy scales, we have $\tilde{k}_1 = 1$ as the position of the first minimum in all cases, while the other minima in $\hat{v}(k)$ are located at selected incommensurate values favoring the stabilization of a selected n -fold quasicrystalline pattern, see Table II for details. To identify the key ingredients in this process, we considered pair interactions with a varying number of minima, i.e., considering cases in which some of the coefficients d_j 's are equal to zero. Once we select a particular minima structure positioned at $\{\tilde{k}_j\}$ in momentum space, the corresponding coefficients $\{d_j\}$ are obtained setting the values of the pair potential at the local minima $\{\hat{v}(\tilde{k}_j)\}$. For all cases considered, we have $g = 10$, $\sigma_j = 0.1$ and $\hat{v}(\tilde{k}_1) = -1$. This choice of dimensionless parameters is consistent with the range

Pattern	\tilde{k}_2	\tilde{k}_3	\tilde{k}_4
8-QC	$2 \cos(\pi/8)$	$2 \cos(3\pi/8)$	$2 \cos(2\pi/8)$
10-QC	$2 \cos(\pi/10)$	$2 \cos(4\pi/10)$	$2 \cos(2\pi/10)$
12-QC	$2 \cos(\pi/12)$	$2 \cos(5\pi/12)$	$2 \cos(3\pi/12)$

Table II. Secondary wave vectors excited in $\hat{v}(k)$ for each quasicrystal structure considered. The patterns n -QC, with $n = 8, 10$ and 12 , correspond to the octagonal, decagonal, and dodecagonal structures, respectively.

of values achievable in current experiments for the contact interaction and intensity of the laser, respectively⁵⁸. For a systematic study, we determine the ground-state phase diagram of the different cases using as running parameters the dimensionless intensity of the pair potential $\lambda^2 U \rho$ and the value of the pair potential at a local minimum $\hat{v}(\tilde{k}_j)$, where \tilde{k}_j represents a selected resonant wave vector of the corresponding structure (see Table II).

B. Superfluid fraction

To deepen our characterization of the quasicrystalline phases, we study the behavior of the superfluid fraction (f_s) in these states. From the knowledge of the ground-state wave function $\psi(\mathbf{r})$ the superfluid fraction can be estimated by means of the Leggett criterion, which provides a lower bound for this quantity. Following well established literature^{69,70} we consider

$$f_s = \text{Max}_\alpha \left[\int_0^L \frac{dx'}{L} \left(\int_0^L \frac{dy'}{L} |\psi'(x', y')|^{-2} \right)^{-1} \right]. \quad (6)$$

In Eq. (6), the prime symbol indicates that the coordinate system is rotated at an angle α with respect to the original coordinate system, consequently $\psi'(x', y') = \psi(x' \cos(\alpha) - y' \sin(\alpha), x' \sin(\alpha) + y' \cos(\alpha))$. As occurs in the case of supersolids⁷¹, the angle α providing the highest value for f_s coincides with the main directions of the structure, which in our case are given by the angles $\alpha_i = 2\pi i/n$, with $i = 0, \dots, n-1$, for an n -fold quasicrystalline phase. Hence, for calculation purposes, we can simply set $\alpha = 0$.

The simultaneous characterization of the superfluid properties and the density pattern allow us to identify different kinds of phases: supersolid states, when superfluidity and a crystalline density pattern coexist, super quasicrystalline states, when the quasicrystal patterns present a finite superfluid fraction, and homogeneous superfluid phases. Moreover, all these phases have their insulating counterparts when the superfluid fraction is close enough to zero^{13,14,72}.

C. Gross-Pitaevskii equation

To verify the results computed within the spectral mean field variational method, we numerically solve the Gross-Pitaevskii^{73,74} equation (GPE) evolved in imaginary time, which provides the ground-state wave function and allows the calculation of the observables of our choice.

The dimensionless GPE evolved in imaginary time $\tau = it$ for the model under consideration reads

$$\frac{\partial \psi(\mathbf{r}, \tau)}{\partial \tau} = \left[\frac{1}{2} \nabla^2 - N \int d\mathbf{r}' v(\mathbf{r} - \mathbf{r}') |\psi(\mathbf{r}', \tau)|^2 \right] \psi(\mathbf{r}, \tau). \quad (7)$$

Eq. (7) is then solved numerically using an adaptive Runge-Kutta method, with a simulation box of linear size $L = 512\lambda$ and discretization $\Delta x = \Delta y = 0.25\lambda$. The non-local term $v_{NL}(\mathbf{r}) = \int d\mathbf{r}' v(\mathbf{r} - \mathbf{r}') |\psi(\mathbf{r}', \tau)|^2$ is computed efficiently with the use of fast-Fourier transformations since $\mathcal{F}[v_{NL}](\mathbf{k}) = \mathcal{F}[v](\mathbf{k}) \mathcal{F}[|\psi|^2](\mathbf{k})$.

As mentioned previously, the ground-state wave function is found as the optimal stationary state of the GPE calculated using a variety of initial conditions. Our initial conditions are given by a droplet on a null background of each modulated pattern considered in our mean field spectral variational analysis placed at the center of our simulation box. When the corresponding pattern is metastable this droplet grows until covering the whole simulation box. If we integrate the GPE for long enough imaginary time a stationary state is achieved. In this way, all the metastable solutions obtained from GPE, which includes the ground state, can be compared with their counter part calculated from the variational approach. For all models considered, we observed a striking agreement between configurations computed in both ways, to show quantitatively such agreement we systematically compare the ground-state superfluid fraction using as inputs these configurations.

III. DODECAGONAL QUASICRYSTAL

To study the stabilization of the dodecagonal quasicrystalline pattern, we begin by considering an effective interaction potential with two length scales. The first minimum in $\hat{v}(k)$ is placed at $k = k_1 = 1$ while the second one is positioned at $k = k_2$, which corresponds to a length scale associated with a resonant wave vector of the dodecagonal structure (see Table II). By fixing the depth of the first minimum to be $\hat{v}(k_1) = -1$, it is possible to study the stabilization of the dodecagonal phase as the vertical position of the second minimum is varied. The form of $\hat{v}(k)$ is shown in Fig. 1(a) for three distinct values of the depth of the second minimum $\hat{v}(\tilde{k}_2)$ and the

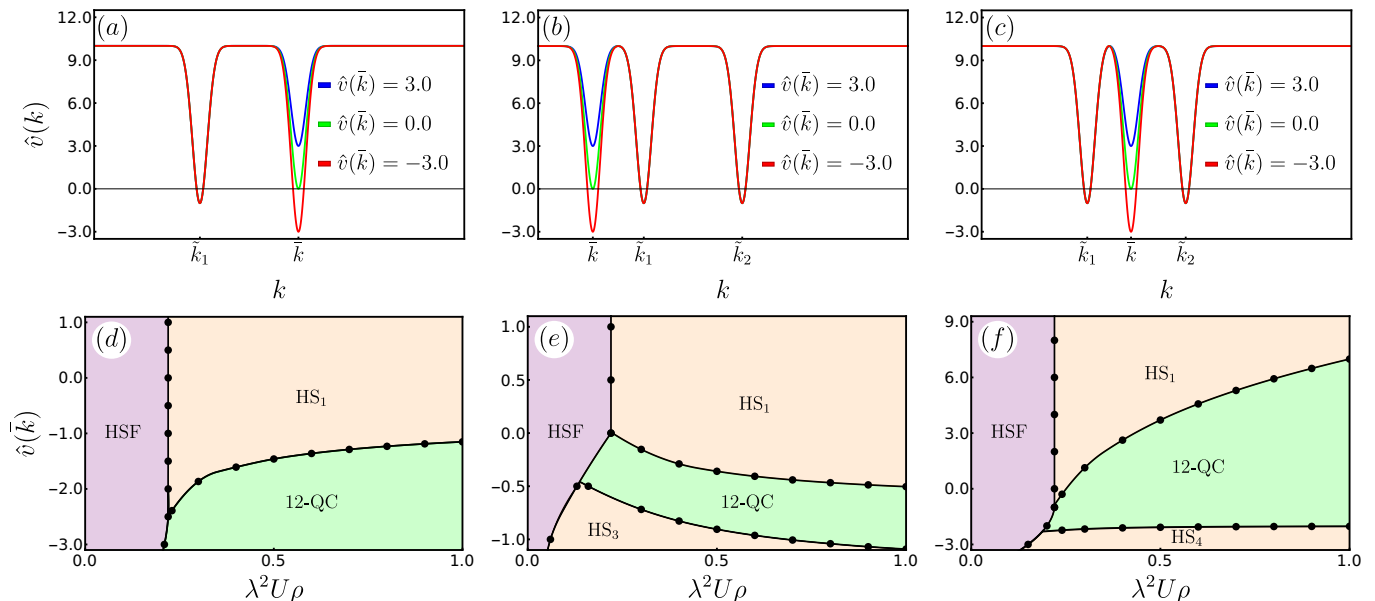


Figure 1. (a)-(c) Pair interaction potential minima structure in Fourier space for the corresponding phase diagrams in (d)-(f), where the first length scale is positioned at $k = \tilde{k}_1 = 1$ and the secondary resonant scales are determined in Table II. Phase diagram for the minima structure associated with the dodecagonal quasicrystal where (d) $\tilde{k} = \tilde{k}_2$ (e) $\tilde{k} = \tilde{k}_3$ and (f) $\tilde{k} = \tilde{k}_4$ indicates the position of the minimum in reciprocal space for which we modify the depth as a parameter to determine the ground state of the system. The acronym HSF stands for homogeneous superfluid, whereas HS and 12-QC stands for hexagonal solid and dodecagonal quasicrystal phases, respectively. The hexagonal states HS_{*i*} refers to a hexagonal phase with characteristic wave vectors dominated by the minimum of $\hat{v}(k)$ at \tilde{k}_i .

corresponding ground-state phase diagram in the $\hat{v}(\tilde{k}_2)$ – $\lambda^2 U \rho$ plane is shown in Fig. 1(d). As can be observed, three different phases are identified, a homogeneous superfluid phase (HSF) at low values of $\lambda^2 U \rho$, a dodecagonal quasicrystal (12-QC) phase for low values of $\hat{v}(\tilde{k}_2)$ and a hexagonal solid phase (HS₁) with characteristic momentum given by \tilde{k}_1 . We notice that the presence of a second minimum at the first resonant wave vector of the dodecagonal structure is sufficient to stabilize such quasicrystalline phase when this minimum is deep enough. However, in the case of a degenerate minima structure, i.e. $\hat{v}(\tilde{k}_1) = \hat{v}(\tilde{k}_2)$, the 12-QC phase is only stabilized at large values of $\lambda^2 U \rho$ in a regime where presumably particles will be largely localized, in agreement with previous works¹³. Moreover, we observe that as the value of the second minimum in $\hat{v}(k)$ is decreased, the transition from the HS₁ phase to the 12-QC phase moves to lower values of $\lambda^2 U \rho$. This behavior is maintained up to the point at which we observe a direct transition from the superfluid to the 12-QC phase.

To further study the stabilization of the 12-QC phase, we modify the interaction potential including a third characteristic length scale manifesting as a minimum in $\hat{v}(k)$ at a resonant wave vector different from \tilde{k}_2 . Here we decided to consider a scenario in which the minima in $\hat{v}(k)$ at $k = \tilde{k}_1$ and $k = \tilde{k}_2$ are degenerate, since this is a quite common assumption for models developing quasicrystalline phases, and investigate the effects of varying the depth of the third minimum added to $\hat{v}(k)$. Firstly,

we examine the situation in which the third minimum is added at $k = \tilde{k}_3$ (see Table II), examples of the resulting pair potential $\hat{v}(k)$ are shown in Fig. 1(b). The corresponding phase diagram in the $\hat{v}(\tilde{k}_3)$ – $\lambda^2 U \rho$ plane is presented in Fig. 1(e). In agreement with the phase diagram obtained for the model with two minima, we observe that the addition of a third minimum not too deep in the pair interaction potential does not produce the stabilization of the 12-QC phase in the range of $\lambda^2 U \rho$ considered. However, when this minimum becomes negative we observe the existence of an interval of values in which the 12-QC phase is again stabilized. Finally, we observe that when the third minimum added is deep enough, a reentrant transition to a new hexagonal phase (HS₃) with characteristic wave vector given by \tilde{k}_3 takes place. This behavior is already expected since an isolated dominant minimum is anticipated to stabilize a hexagonal ground state.

Lastly, we consider the excitation of a third minimum at the remaining wave vector belonging to the first generation of resonant wave vectors of the dodecagonal quasicrystal, the one with $k = \tilde{k}_4$ (see Table II). In this scenario, the interaction potential takes the form depicted in Fig. 1(c) and the corresponding ground-state phase diagram varying $\hat{v}(\tilde{k}_4)$ is shown in Fig. 1(f). As can be observed, the addition of this third length scale is much more effective in promoting the stabilization of the quasicrystalline phase when compared to the scenario shown in Fig. 1(e). In this case, even the addition of a positive

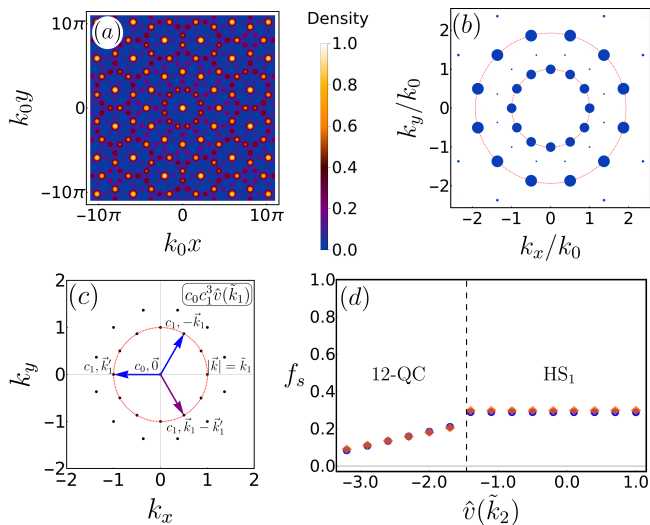


Figure 2. (a) Real space mapping for the dodecagonal structure in the phase diagram of Fig. 1(d) for parameter values $\hat{v}(\tilde{k}_2) = -2.30$ and $\lambda^2 U \rho = 0.50$ and its corresponding (b) diffraction pattern. The red circles indicate the two minima and the size of the Fourier modes in blue disks is scaled by a linear function, where the zero harmonic mode has been omitted. (c) Most relevant energy contributions to the total energy of the quasicrystalline structures as a contraction in the $\tilde{k}_1 = 1$ layer for the dodecagonal vectors. (d) Superfluid fraction for a fixed density value $\lambda^2 U \rho = 0.50$ in the dodecagonal quasicrystal for the ground state depicted in Fig. 1(d). The blue points represent the superfluid fraction obtained via mean field spectral variational method while the orange diamonds are determined via the solution of the GPE.

minimum with a relative high value already induces the stabilization of the 12-QC for moderate values of $\lambda^2 U \rho$. As expected, the strongest effect is achieved when the minimum is negative and in this case the preemptive hexagonal phase HS₁ is not present and we have a direct transition from the HSF to the 12-QC phase when $\lambda^2 U \rho$ is increased. Moreover, as in the previous case, a further decrease of $\hat{v}(\tilde{k}_4)$ eventually promotes a transition to the HS₄ phase with characteristic wave vector close to \tilde{k}_4 .

The three scenarios discussed above show different routes for the stabilization of the 12-QC phase in two-dimensional bosonic gases. Although, in this case, the presence of two properly positioned minima is enough for such stabilization, differently from the classical case^{10,45}, it requires a second high-momentum minimum much deeper than the first one to stabilize the 12-QC phase in the low $\lambda^2 U \rho$ regime. Alternatively, the addition of a third minimum to $\hat{v}(k)$ at \tilde{k}_3 or \tilde{k}_4 enhance significantly the stability of the 12-QC phase, even allowing us to observe this phase with a degenerate pair potential ($\hat{v}(\tilde{k}_1) = \hat{v}(\tilde{k}_2)$). In this sense, by comparing Fig. 1(e) and Fig. 1(f) we conclude that in order to enhance the stability of the 12-QC phase, it is more effective to decrease $\hat{v}(\tilde{k}_4)$ than $\hat{v}(\tilde{k}_3)$.

Regarding the structural properties of the 12-QC phase, as an example, we consider the scenario presented in Fig. 1(a) with parameters $\hat{v}(\tilde{k}_2) = -2.30$ and $\lambda^2 U \rho = 0.50$. In Fig. 2(a), we show the ground-state density pattern obtained after the energy minimization, and in Fig. 2(b) a graphic of the corresponding Fourier transform of the solution. The radii of the circles are proportional to the modulus of the Fourier amplitudes, excluding the circle corresponding to the $k = 0$ Fourier mode, which is not presented. The red circumferences indicate the position of the minima of $\hat{v}(k)$ in this case. As can be observed, the presence of the minima in $\hat{v}(k)$ controls which are the main modes excited in the quasicrystalline density pattern, this kind of phenomenology was verified in all scenarios considered in this work.

To better understand the process of stabilization of the dodecagonal pattern and the greater stability of this structure in comparison with other quasicrystalline phases, as we will see later, we consider a simplified two-mode expansion including only the two main modes of the structure with $|\mathbf{k}_j| = \{\tilde{k}_1, \tilde{k}_2\}$, as it is the case in Fig. 1(a). Our goal here is to assess the relative importance of the various interactions present in the energy per particle functional. Replacing Eq. (4) into Eq. (3) we can obtain the general expression:

$$\frac{E[\psi]}{N} = \frac{1}{8Z} \sum_j \mathbf{k}_j^2 |c(\mathbf{k}_j)|^2 + \frac{\lambda^2 U \rho}{32Z^2} \sum_{j,l,m} c(\mathbf{k}_j) c(\mathbf{k}_j + \mathbf{k}_l)^* \times c(\mathbf{k}_m) c(\mathbf{k}_m - \mathbf{k}_l)^* \hat{v}(\mathbf{k}_l), \quad (8)$$

where $Z = \frac{1}{4} \sum_j c(\mathbf{k}_j)^2$ and $c(0) = 2$. This expression is general and naturally remains valid for the two mode ansatz under consideration. As we can observe from Eq. (8), the potential energy contribution is given as a sum of contractions of four Fourier amplitudes paired carrying momentum \mathbf{k}_l and $-\mathbf{k}_l$. At this point, it is possible to identify which contractions produces the highest contributions to the potential energy and hence the leading mechanisms of stabilization of a given quasicrystalline phase. The most relevant type of contraction is naturally the one of the form $c(\mathbf{0}) c(\mathbf{k}_1)^* c(\mathbf{0}) c(-\mathbf{k}_1)^* \hat{v}(\mathbf{k}_1)$ and its equivalents. However, this kind of contraction is present in the energy per particle of all the solutions considered due to their pattern inversion symmetry. The next most relevant contribution, which is only present for solutions with symmetry against rotations of $\pi/3$, are of the type $c(\mathbf{0}) c(\mathbf{k}_1)^* c(\mathbf{k}'_1) c(\mathbf{k}'_1 - \mathbf{k}_1)^* \hat{v}(\mathbf{k}_1)$, where the vectors \mathbf{k}_1 and \mathbf{k}'_1 are of equal modulus ($|\mathbf{k}_1| = |\mathbf{k}'_1|$) and form an angle of $\pi/3$ between them. As we can see, this is a contribution combining one zero-momentum Fourier amplitude with three amplitudes corresponding to vectors in the same shell, see Fig. 2(c) for a pictorial representation of the corresponding contraction. In all the tests performed, this kind of term was responsible for around 40% of the total energy of the reduced expansion for the dodecagonal pattern explaining the great stability of this phase in comparison to other quasicrystal so-

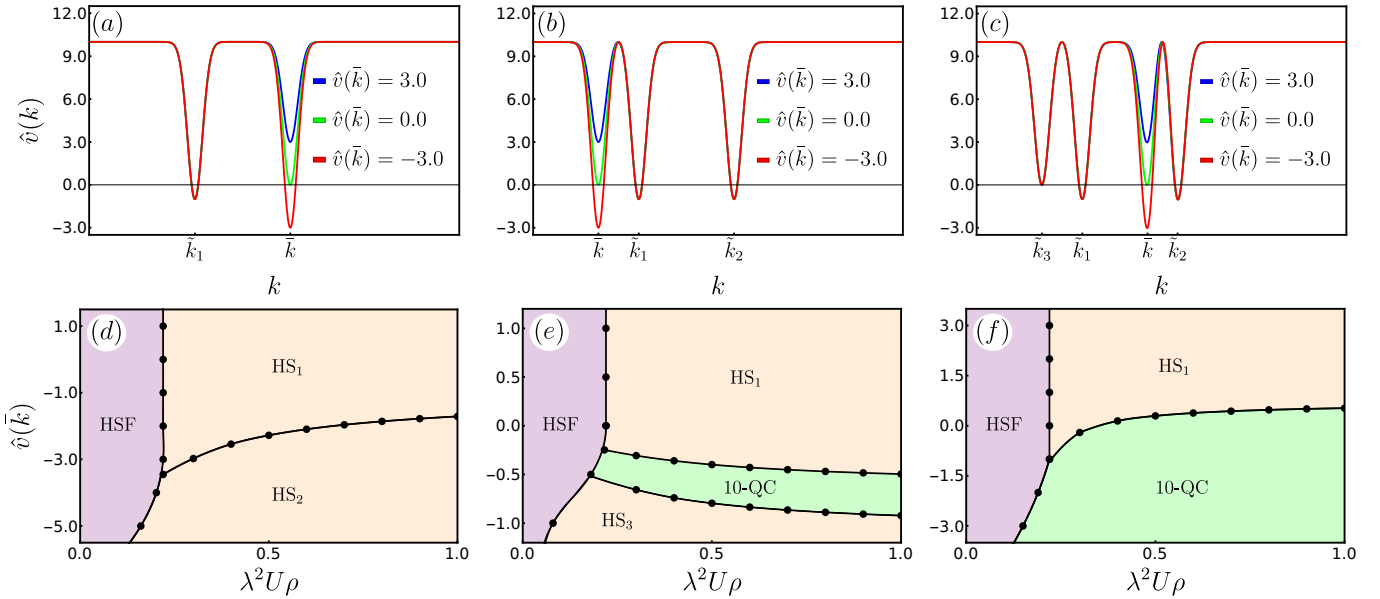


Figure 3. (a)-(c) Pair interaction potential minima structure in Fourier space for the corresponding phase diagrams in (d)-(f), in which the first length scale is positioned at $k = \tilde{k}_1 = 1$ and the secondary resonant scales are determined in Table II. Phase diagram for the minima structure associated with the decagonal quasicrystal where (d) $\tilde{k} = \tilde{k}_2$ (e) $\tilde{k} = \tilde{k}_3$ and (f) $\tilde{k} = \tilde{k}_4$ indicates the position of the minimum in reciprocal space for which we modify the depth as a parameter to determine the ground state of the system. The notation employed to label the phases is analogous to the one established in Fig.1.

lutions that do not contain such interaction terms.

Moreover, we investigate how the superfluid properties of the 12-QC phase are impacted by the properties of the pair interaction potential. We estimate the superfluid fraction by means of the Legget's criterion and consider the scenario posed by Fig. 1(a). The superfluid fraction is calculated across a vertical line of the phase diagram of Fig. 1(d), specifically we consider $\lambda^2 U \rho = 0.50$ and use $\hat{v}(\tilde{k}_2)$ as the running parameter. The results are shown in Fig. 2(d), where the blue points corresponds to the values of the superfluid fraction obtained from the density profile calculated using the mean field spectral variational method while the orange diamonds corresponds to the profile determined via the GPE solution. Within the HS₁ phase, for $\hat{v}(\tilde{k}_2) \gtrsim -1.5$, we observe a superfluid fraction essentially constant. This is explained by the fact that Fourier modes with $|\mathbf{k}| = \tilde{k}_2$ are not present in the HS₁ state when the characteristic wave vector of the pattern is of the order of \tilde{k}_1 . Moreover, the fact that superfluidity is significant along this phase allows us to conclude that it is actually a supersolid phase. On the other hand, in the region in which the model displays a 12-QC phase, we can notice how the increase of the depth of the second minimum decreases the superfluid fraction. This occurs because decreasing the energy cost of the second minimum promotes higher Fourier amplitudes which implies in a more localized quasicrystalline density pattern, hindering superfluidity in the system. Nonetheless, despite the tendency of the superfluidity, within the quasicrystalline phase its value is still significant, allowing us to confirm that this phase is actually a superfluid dodecago-

nal phase.

IV. DECAGONAL QUASICRYSTAL

Now we proceed to study the stabilization of the decagonal quasicrystal (10-QC) phase. We explore systematically pair potentials with multiple length scales in the form of several minima in $\hat{v}(k)$, positioned to enhance the stability of this structure. Naturally, the first model to be considered contains two minima, the first one at $k = \tilde{k}_1 = 1$ and the second one at $k = \tilde{k}_2$ (see Table II). The corresponding pair interaction potential is displayed in Fig. 3(a), while the associated ground-state phase diagram is shown in Fig. 3(d). In this case, a phase transition is observed at moderate and high intensity of the pair potential $\lambda^2 U \rho$ as the vertical position of the high momentum minima is varied. For low enough values of $\hat{v}(\tilde{k}_2)$, the system display a transition between two hexagonal solid phases in which the characteristic wave vector of the patterns changes from \tilde{k}_1 (HS₁) to \tilde{k}_2 (HS₂). Interestingly, despite the fact that this model produce the excitation of the two main wave vectors of the decagonal quasicrystal, this pair potential configuration is still favorable to the hexagonal structure even when the high momentum minimum dominates. This indicates the necessity of introducing additional minima in $\hat{v}(k)$ to achieve the stabilization of the decagonal quasicrystal pattern.

To proceed we consider the case in which a third minimum in $k = \tilde{k}_3$ (see Table II) is added to a two min-

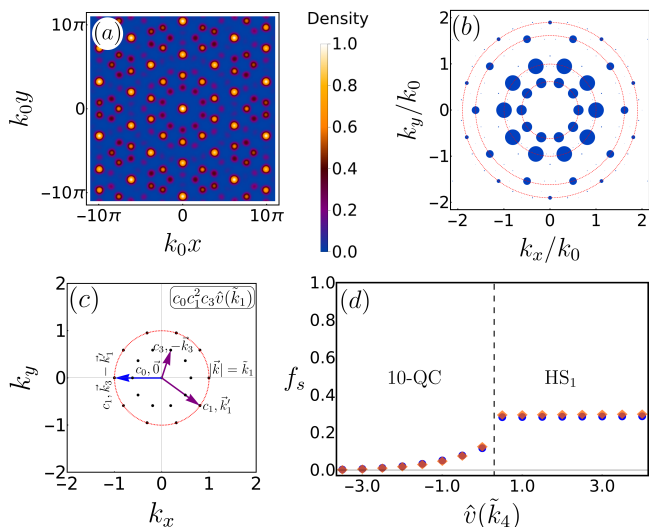


Figure 4. (a) Real space mapping for the decagonal structure in the phase diagram of Fig. 3(f) for parameter values $\hat{v}(\tilde{k}_4) = -1.50$ and $\lambda^2 U \rho = 0.50$ and its corresponding (b) diffraction pattern. The red circles indicates the two minima and the size of the Fourier modes in blue disks is scaled by a linear function, where the zero harmonic mode has been omitted. (c) Most relevant energy contributions to the total energy of the quasicrystalline structures as a contraction in the $k_1 = 1$ layer for the decagonal vectors. (d) Superfluid fraction for a fixed density value $\lambda^2 U \rho = 0.50$ in the decagonal quasicrystal for the ground state depicted in Figure 3(f). The blue points represents the superfluid fraction obtained via mean field spectral variational method while the orange diamonds are determined via GPE simulations.

ima degenerate potential with $\hat{v}(\tilde{k}_1) = \hat{v}(\tilde{k}_2) = -1$. The resulting model for $\hat{v}(k)$ can be observed in Fig. 3(b) and the corresponding ground-state phase diagram using as running parameters the $\hat{v}(\tilde{k}_3)$ and $\lambda^2 U \rho$ is shown in Fig. 3(e). As can be noticed, the introduction of a third characteristic length scale allows the stabilization of a 10-QC phase for a certain range of $\hat{v}(\tilde{k}_3)$. Interestingly, if $\hat{v}(\tilde{k}_3)$ is deep enough the system reenters into a hexagonal phase (HS₃) with characteristic wave vector \tilde{k}_3 . Moreover, the quasicrystal phase exists up to the low intensity potential regime, making the system to present a direct transition from the homogeneous to the quasicrystal phase. However, this behavior is only present in a limited region of $\hat{v}(\tilde{k}_3)$, raising naturally the question about what can be done to enhance further the stability or extension of this phase within the phase diagram.

In order to answer this question, it is natural to consider the introduction of an additional length scale in the form of a minimum in $\hat{v}(k)$ at the remaining characteristic wave vector of the decagonal quasicrystalline structure. In this way, we add a minimum at $k = \tilde{k}_4$ (see Table II) to a three minima potential that does not display a quasicrystal phase at any intensity ($\lambda^2 U \rho$) of the pair potential. In terms of minima position, this model satisfy $\hat{v}(\tilde{k}_1) = \hat{v}(\tilde{k}_2) = -1$, $\hat{v}(\tilde{k}_3) = 0$ and $\hat{v}(\tilde{k}_4)$ is taken as run-

ning parameter for the construction of the corresponding phase diagram. The typical form of this kind of pair potential is displayed in Fig. 3(c), while in Fig. 3(f) we present the corresponding ground-state phase diagram obtained. As can be observed, when the depth of the fourth minimum at \tilde{k}_4 is increased the system transitions from a HS₁ to a 10-QC phase. This means that only the addition of this extra minimum promotes the stabilization of the 10-QC phase, but the extension of the quasicrystal phase is greatly enhanced.

To deepen our understanding about the 10-QC phase, we now focus on its structural properties. In Fig. 4(a) and (b), we present a typical density pattern configuration and its corresponding Fourier transform for a pair potential of the type presented in Fig. 3(c) ($\hat{v}(\tilde{k}_4) = -1.50$ and $\lambda^2 U \rho = 0.50$). The radius of each circle in the Fourier transform plot is proportional to the corresponding Fourier amplitude. As we can see, the main modes excited in the density pattern corresponds to those promoted by the minima structure of the pair potential as in the case of the 12-QC phase. An analysis of the potential energy contractions leading to dominant contributions, analogous to the one performed in the case of the dodecagonal structure, reveals that this structure does not have exclusive amplitude contractions which are specially impactful as in the previous case considered. In this case, contractions allowed for all quasicrystal structures, such as the one depicted in Fig. 4(c) for the decagonal pattern, are the leading contribution in the potential energy expansion.

The behavior of the superfluid fraction for the model in Fig. 3(c), keeping $\lambda^2 U \rho = 0.50$ and using $\hat{v}(\tilde{k}_4)$ as our running parameter, is shown in Fig. 4(d). We can observe that within the region corresponding to the HS₁ phase, modifying $\hat{v}(\tilde{k}_4)$ does not affect the superfluid fraction. As previously observed, since \tilde{k}_4 does not match any resonant momentum of the hexagonal crystal solution with characteristic momentum \tilde{k}_1 , the hexagonal ground state is not affected by variations of $\hat{v}(\tilde{k}_4)$ and hence neither the superfluid fraction. On the other hand, when the system transitions to the decagonal phase, we observe that making deeper the minimum at \tilde{k}_4 results in a decrease of the superfluid fraction. This behavior is a consequence of increasing the stability of the quasicrystalline phase, which results in an increase of the quasicrystal Fourier amplitudes. This in turn reflects on a more localized density profiles which hinder superfluidity. Moreover, it is interesting to notice that close to the quasicrystal phase boundary, the superfluid fraction takes significant values, indicating the existence of a superfluid decagonal phase.

V. OCTAGONAL QUASICRYSTAL

Finally, we focus on the study of the stability of the octagonal quasicrystal (8-QC) phase. As in the previous cases, we initially consider a two minima model with a first minimum positioned at $\tilde{k}_1 = 1$ with $\hat{v}(\tilde{k}_1) = -1$ and

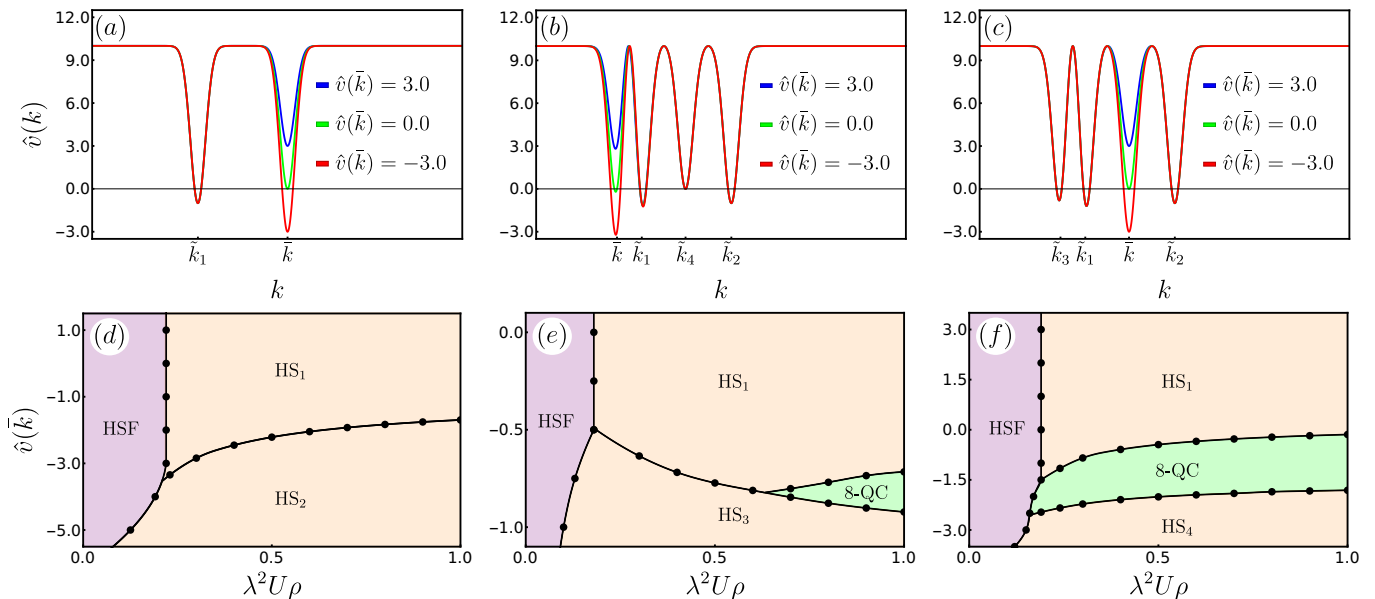


Figure 5. (a)-(c) Pair interaction potential minima structure in Fourier space for the corresponding phase diagrams in (d)-(f), where the first length scale is positioned at $k = \tilde{k}_1 = 1$ and the secondary resonant scales are determined in Table II. Phase diagram for the minima structure associated with the octagonal quasicrystal where (d) $k = \tilde{k}_2$ (e) $k = \tilde{k}_3$ and (f) $k = \tilde{k}_4$ indicates the position of the minimum in reciprocal space for which we modify the depth as a parameter to determine the ground state of the system. The notation employed to label the phases is analogous to the one established in Fig.1.

a second minimum at \tilde{k}_2 (see Table II) with a varying vertical position, as it is shown in Fig. 5(a). The resulting phase diagram for this model is shown in Fig. 5(d). The obtained phase diagram presents the trivial homogeneous superfluid phase for low values of $\lambda^2 U \rho$ and a phase transition from a hexagonal phase with characteristic wave vector \tilde{k}_1 (HS₁) to one with characteristic wave vector \tilde{k}_2 (HS₂) as $\hat{v}(\tilde{k}_2)$ is decreased. Interestingly, the addition of a third resonant length scale of the 8-QC phase to the pair potential $\hat{v}(k)$, either $k = \tilde{k}_3$ or $k = \tilde{k}_4$, in a scenario with two degenerate minima is not sufficient for the stabilization of the 8-QC phase as occurs in the case of the decagonal pattern, see Fig. 4(e). Even in a scenario without any degeneracy we did not observe the stabilization of the 8-QC pattern using only potentials with three characteristic length scales.

In this way we proceed by allowing the existence of a fourth minimum in $\hat{v}(k)$. Hence, our pair potential have local minima at $k = \tilde{k}_1, \tilde{k}_2, \tilde{k}_3$ and \tilde{k}_4 , see table II. For this kind of model, we set $\hat{v}(\tilde{k}_1)$ and $\hat{v}(\tilde{k}_2)$ as degenerate minima, while we explore separately the phase diagram varying the vertical position of the other two minima present in $\hat{v}(k)$. Firstly, we set $\hat{v}(\tilde{k}_4) = 0$ and vary the depth of the minimum at \tilde{k}_3 . The resulting model is presented in Fig. 5(b) and the corresponding phase diagram is shown in Fig. 5(e). Here we observe that in the low $\lambda^2 U \rho$ regime, the system has a similar behavior to the two-minima model presented in Fig. 5(a), with the HS₃ phase having characteristic momentum k_3 . However, for large enough potential intensity we observe

the stabilization of an 8-QC in a narrow range of $\hat{v}(\tilde{k}_3)$. Although, strictly speaking the 8-QC exist as the ground state of this model, its stabilization occurs in a region where the validity of the mean field approximation itself can be questioned as the intensity of the pair potential in this region can be hardly considered as weak.

In the last possible scenario, we explore a four-minima interaction potential fixing $\hat{v}(\tilde{k}_3) = -0.6$, a value that in principle favors the formation of the octagonal quasicrystal without turning this minimum the dominant one, see Fig. 5(c). Meanwhile, we use the depth of the minimum at $k = \tilde{k}_4$ as running parameter for the construction of the phase diagram displayed in Fig. 5(f). As can be observed, this last family of models greatly enhance the stability of the 8-QC phase. This is evident since, in this case, there is a significant range of $\hat{v}(\tilde{k}_4)$ for which we have a direct transition from the homogeneous to the 8-QC phase increasing the potential intensity. Moreover, the system naturally displays a HS₄ phase with characteristic momentum close to \tilde{k}_4 when the potential minimum at this momentum is deep enough. The systematic study presented allow us to conclude that in order to stabilize the 8-QC phase for the model considered, at least four characteristic wave vectors of this structure should be excited by the pair interaction potential $\hat{v}(k)$. Interestingly, the value of $\hat{v}(\tilde{k}_4)$ seem to have a much stronger impact enhancing stability of the 8-QC than the value of $\hat{v}(\tilde{k}_3)$.

A real space density configuration example and its corresponding Fourier transform plot, for the model in Fig. 5(c), are presented in Fig. 6(a) and (b), respectively.

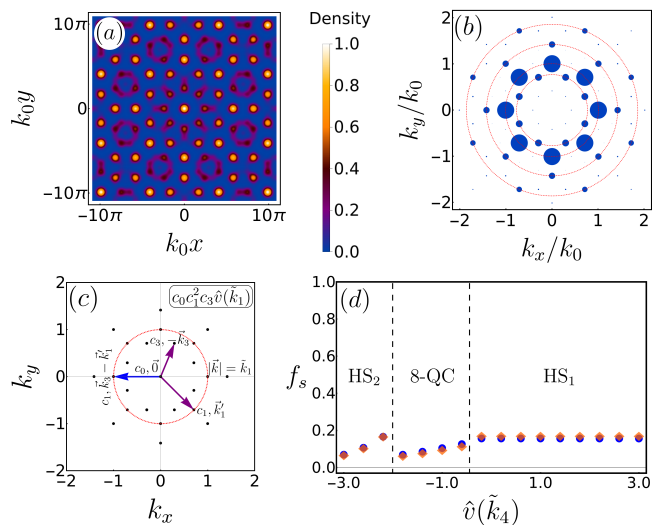


Figure 6. (a) Real space mapping for the octagonal structure in the phase diagram of Fig. 5(f) for parameter values $\hat{v}(\tilde{k}_4) = -1.25$ and $\lambda^2 U \rho = 0.50$ and its corresponding (b) diffraction pattern. The red circles indicate the two minima and the size of the Fourier modes in blue disks is scaled by a linear function, where the zero harmonic mode has been omitted. (c) Most relevant energy contributions to the total energy of the quasicrystalline structures as a contraction in the $k_1 = 1$ layer for the octagonal vectors. (d) Superfluid fraction for a fixed density value $\lambda^2 U \rho = 0.50$ in the octagonal quasicrystal for the ground state depicted in Fig. 5(f). The blue points represent the superfluid fraction obtained via mean field spectral variational method while the orange diamonds are determined via GPE simulations.

The parameters employed for the variational minimization are $\hat{v}(\tilde{k}_4) = -1.25$ and $\lambda^2 U \rho = 0.50$. It is worth noticing how the stabilization of 8-QC phase occurs when all the unstable momenta of the engineered pair potential are excited in the density pattern of the system. Moreover, the investigation of the energy behavior using a reduced Fourier expansion for the 8-QC reveals a scenario similar to the one observed for the 10-QC, where no exclusive form of contraction has a high impact on the energy values and, in this context, only the introduction of additional modes and the eventual emergence of new contractions with higher momentum are effective in the stabilization of the 8-QC phase. We show in Fig. 6(c) an example of the leading contractions for this phase, the specific wave vectors employed for such contractions can switch depending on which is the most unstable wave vector in the system, however preserving the rule of having two modes excited at the most unstable momenta of the system, one at the second most unstable momenta and one with zero momentum.

For completeness, we finally study the behavior of the superfluid fraction for the model described in Fig. 5(c) and Fig. 5(f), using $\hat{v}(\tilde{k}_4)$ as running parameter and fixing $\lambda^2 U \rho = 0.50$. The results obtained are displayed in Fig. 6(d). As previously observed, since the HS₁

phase does not excite Fourier modes with momentum \tilde{k}_4 or close to it, this phase is unaffected by changes in $\hat{v}(\tilde{k}_4)$. In turn, when the system transitions to a phase in which Fourier modes with momentum \tilde{k}_4 , or close to it, are excited, to decrease the value of $\hat{v}(\tilde{k}_4)$ promote localization of the density pattern, as explained in previous cases. This is the reason for the observed decreasing behavior of the superfluid fraction as we decrease the value of $\hat{v}(\tilde{k}_4)$ for the 8-QC and the HS₄ phase, respectively. Moreover, we can notice that as in previous cases, also the 8-QC phase is able to host significant superfluidity confirming the existence of a superfluid octagonal phase.

VI. FINAL REMARKS

In this work, we systematically studied the necessary conditions for the stabilization of eight-, ten- and twelve-fold self-organized quantum quasicrystals. Unlike the classical scenario, we found that quantum quasicrystals with distinct rotational symmetries need pair interaction potentials with a different number of properly selected unstable wave vectors. In the case of the dodecagonal quasicrystal, a two negative minima potential is enough for the stabilization, as previously pointed out in the literature⁴⁸. Meanwhile, the decagonal and octagonal quasicrystal structures need pair interaction potentials with at least three and four minima negative minima properly engineered to be stabilized, respectively. The greater stability of the dodecagonal quasicrystal with respect to other quasicrystalline structures considered resides in the geometric property of having six-fold rotational symmetry. Ultimately, this property is responsible for the existence of Fourier-mode triplets with wave vectors of equal modulus that adds up to zero. As occurs in hexagonal crystals, this feature is responsible for cubic potential energy contributions with a significant impact on decreasing the total energy cost of phases that share this symmetry, see Section III. Moreover, as can be observed in Fig. 1(f), Fig. 3(f) and Fig. 5(f), all quasicrystalline phases studied have a sector in which the superfluid fraction is significant, allowing us to conclude that these are actually super quasicrystal phases. These results were confirmed by extensive Gross-Pitaevskii computations, which produce equivalent configuration and superfluid fraction to those obtained with our variational spectral approach.

We believe that the present results are relevant for the investigation of quasicrystal structures produced in cavity mediated interacting Bose-Einstein condensates^{55,75–77}. The design on demand of cavity mediated interactions have paved a way to investigate a variety of cutting-edge many-body phases. In this regard, such systems show the interesting opportunity to operate with lattice phononic modes, a flexible manner to test quasicrystals in a quantum framework. At the same time, the

interplay between long-range magnetic and light-induced interactions in a Bose-Einstein condensate⁷⁸ is another promising experimental setup that, in principle, should observe 8-QC, 10-QC and 12-QC patterns displaying a finite superfluid signal. Especially relevant is also the usage of dipolar atoms in cavities⁷⁹, allowing the implementation of many-body systems with highly tunable interactions capable of producing self-assembled quasicrystal clusters. Here it will be of key importance to inspect the stability of octagonal as well as decagonal phases.

VII. ACKNOWLEDGMENTS

A.M.C. acknowledge UNIFI for financial support and hospitality. This work was supported by the European

Union through the Next Generation EU funds through the Italian MUR National Recovery and Resilience Plan, Mission 4 Component 2–Investment 1.4–National Center for HPC, Big Data and Quantum Computing (CUP Grant No. B83C22002830001). F. C. and V. Z. acknowledge financial support from PNRR Ministero Università e Ricerca Project No. PE0000023-NQSTI funded by European Union-Next-Generation EU. The numerical solution of the GPE was performed using the XMDS2 software⁸⁰.

-
- ¹ T. Neuhaus and C. N. Likos, *Journal of Physics: Condensed Matter* **23**, 234112 (2011).
- ² F. Cinti, T. Macrì, W. Lechner, G. Pupillo, and T. Pohl, *Nature Communications* **5**, 3235 (2014).
- ³ M. de Mello, R. Díaz-Méndez, and A. Mendoza-Coto, *Entropy* **25** (2023), 10.3390/e25020356.
- ⁴ A. Mendoza-Coto, D. d. S. Caetano, and R. Díaz-Méndez, *Phys. Rev. A* **104**, 013301 (2021).
- ⁵ D. Shechtman, I. Blech, D. Gratias, and J. W. Cahn, *Phys. Rev. Lett.* **53**, 1951 (1984).
- ⁶ M. Engel and H.-R. Trebin, *Phys. Rev. Lett.* **98**, 225505 (2007).
- ⁷ D. V. Talapin, E. V. Shevchenko, M. I. Bodnarchuk, X. Ye, J. Chen, and C. B. Murray, *Nature* **461**, 964 (2009).
- ⁸ S. Fischer, A. Exner, K. Zielske, J. Perlich, S. Deloudi, W. Steurer, P. Lindner, and S. Förster, *Proceedings of the National Academy of Sciences* **108**, 1810 (2011).
- ⁹ N. A. Wasio, R. C. Quardokus, R. P. Forrest, C. S. Lent, S. A. Corcelli, J. A. Christie, K. W. Henderson, and S. A. Kandel, *Nature* **507**, 86 (2014).
- ¹⁰ K. Barkan, M. Engel, and R. Lifshitz, *Phys. Rev. Lett.* **113**, 098304 (2014).
- ¹¹ T. Dotera, T. Oshiro, and P. Zihler, *Nature* **506**, 208 (2014).
- ¹² G. Pupillo, P. c. v. Zihler, and F. Cinti, *Phys. Rev. B* **101**, 134522 (2020).
- ¹³ A. Mendoza-Coto, R. Turcati, V. Zampronio, R. Díaz-Méndez, T. Macrì, and F. Cinti, *Phys. Rev. B* **105**, 134521 (2022).
- ¹⁴ M. Grossklags, M. Ciardi, V. Zampronio, F. Cinti, and A. Mendoza-Coto, *Results in Physics* **65**, 107991 (2024).
- ¹⁵ F. Cinti, P. Jain, M. Boninsegni, A. Micheli, P. Zoller, and G. Pupillo, *Phys. Rev. Lett.* **105**, 135301 (2010).
- ¹⁶ Y.-C. Zhang, F. Maucher, and T. Pohl, *Phys. Rev. Lett.* **123**, 015301 (2019).
- ¹⁷ F. Böttcher, J.-N. Schmidt, M. Wenzel, J. Hertkorn, M. Guo, T. Langen, and T. Pfau, *Phys. Rev. X* **9**, 011051 (2019).
- ¹⁸ L. Tanzi, E. Lucioni, F. Famà, J. Catani, A. Fioretti, C. Gabbanini, R. N. Bisset, L. Santos, and G. Modugno, *Phys. Rev. Lett.* **122**, 130405 (2019).
- ¹⁹ L. Chomaz, D. Petter, P. Ilzhöfer, G. Natale, A. Trautmann, C. Politi, G. Durastante, R. M. W. van Bijnen, A. Patscheider, M. Sohmen, M. J. Mark, and F. Ferlaino, *Phys. Rev. X* **9**, 021012 (2019).
- ²⁰ P. B. Blakie, D. Baillie, L. Chomaz, and F. Ferlaino, *Phys. Rev. Res.* **2**, 043318 (2020).
- ²¹ E. Berg, E. Fradkin, E.-A. Kim, S. A. Kivelson, V. Oganesyan, J. M. Tranquada, and S. C. Zhang, *Phys. Rev. Lett.* **99**, 127003 (2007).
- ²² D. G. Barci, A. Mendoza-Coto, and D. A. Stariolo, *Phys. Rev. E* **88**, 062140 (2013).
- ²³ A. Mendoza-Coto, D. A. Stariolo, and L. Nicolao, *Phys. Rev. Lett.* **114**, 116101 (2015).
- ²⁴ R. M. W. van Bijnen and T. Pohl, *Phys. Rev. Lett.* **114**, 243002 (2015).
- ²⁵ A. Mendoza-Coto, D. G. Barci, and D. A. Stariolo, *Phys. Rev. B* **95**, 144209 (2017).
- ²⁶ A. Mendoza-Coto, D. E. B. de Oliveira, L. Nicolao, and R. Díaz-Méndez, *Phys. Rev. B* **101**, 174438 (2020).
- ²⁷ L. Radzihovsky, *Phys. Rev. Lett.* **125**, 267601 (2020).
- ²⁸ S. Prestipino and F. Saija, *The Journal of Chemical Physics* **141**, 184502 (2014).
- ²⁹ S. Prestipino, A. Sergi, and E. Bruno, *Phys. Rev. B* **98**, 104104 (2018).
- ³⁰ A. Mendoza-Coto, R. Cenci, G. Pupillo, R. Díaz-Méndez, and E. Babaev, *Soft Matter* **17**, 915 (2021).
- ³¹ N. Podoliak, P. Salamon, L. Lejček, P. Kužel, and V. Novotná, *Phys. Rev. Lett.* **131**, 228101 (2023).
- ³² J. Xia and Y. Han, *Phys. Rev. Res.* **6**, 033232 (2024).
- ³³ A. Bianconi, *International Journal of Modern Physics B* **14**, 3289 (2000).
- ³⁴ A. Bianconi, D. Di Castro, N. Saini, and G. Bianconi, “Superstripes,” in *Phase Transitions and Self-Organization in Electronic and Molecular Networks*, edited by M. F. Thorpe and J. C. Phillips (Springer US, Boston, MA, 2001) pp. 375–388.
- ³⁵ R. Díaz-Méndez, A. Mendoza-Coto, R. Mulet, L. Nicolao, and D. A. Stariolo, *The European Physical Journal B* **81**, 309 (2011).
- ³⁶ R. M. Fernandes, A. V. Chubukov, J. Knolle, I. Eremin, and J. Schmalian, *Phys. Rev. B* **85**, 024534 (2012).

- ³⁷ A. Mendoza-Coto and D. A. Stariolo, *Phys. Rev. E* **86**, 051130 (2012).
- ³⁸ R. M. Fernandes, A. V. Chubukov, and J. Schmalian, *Nature Physics* **10**, 97 (2014).
- ³⁹ A. Mendoza-Coto, O. V. Billoni, S. A. Cannas, and D. A. Stariolo, *Phys. Rev. B* **94**, 054404 (2016).
- ⁴⁰ A. Mendoza-Coto, L. Nicolao, and R. Díaz-Méndez, *Scientific Reports* **9**, 2020 (2019).
- ⁴¹ D. Levine and P. J. Steinhardt, *Phys. Rev. B* **34**, 596 (1986).
- ⁴² J. E. S. Socolar, T. C. Lubensky, and P. J. Steinhardt, *Phys. Rev. B* **34**, 3345 (1986).
- ⁴³ R. Lifshitz, *Israel Journal of Chemistry* **51**, 1156 (2011).
- ⁴⁴ X. Zeng, G. Ungar, Y. Liu, V. Percec, A. E. Dulcey, and J. K. Hobbs, *Nature* **428**, 157 (2004).
- ⁴⁵ T. Dotera, *Israel Journal of Chemistry* **51**, 1197 (2011).
- ⁴⁶ K. Jiang, P. Zhang, and A.-C. Shi, *Journal of Physics: Condensed Matter* **29**, 124003 (2017).
- ⁴⁷ M. Ciardi, A. Angelone, F. Mezzacapo, and F. Cinti, *Phys. Rev. Lett.* **131**, 173402 (2023).
- ⁴⁸ V. Heinonen, K. J. Burns, and J. Dunkel, *Phys. Rev. A* **99**, 063621 (2019).
- ⁴⁹ S. Gopalakrishnan, B. L. Lev, and P. M. Goldbart, *Nature Physics* **5**, 845 (2009).
- ⁵⁰ S. Gopalakrishnan, B. L. Lev, and P. M. Goldbart, *Phys. Rev. A* **82**, 043612 (2010).
- ⁵¹ V. D. Vaidya, Y. Guo, R. M. Kroeze, K. E. Ballantine, A. J. Kollár, J. Keeling, and B. L. Lev, *Phys. Rev. X* **8**, 011002 (2018).
- ⁵² T. D. Farokh Mivehvar, Francesco Piazza and H. Ritsch, *Advances in Physics* **70**, 1 (2021).
- ⁵³ Y.-C. Zhang, V. Walther, and T. Pohl, *Phys. Rev. A* **103**, 023308 (2021).
- ⁵⁴ P. Karpov and F. Piazza, *Phys. Rev. Lett.* **128**, 103201 (2022).
- ⁵⁵ F. Mivehvar, H. Ritsch, and F. Piazza, *Phys. Rev. Lett.* **123**, 210604 (2019).
- ⁵⁶ Y. Guo, R. M. Kroeze, V. D. Vaidya, J. Keeling, and B. L. Lev, *Phys. Rev. Lett.* **122**, 193601 (2019).
- ⁵⁷ Y. Guo, R. M. Kroeze, B. P. Marsh, S. Gopalakrishnan, J. Keeling, and B. L. Lev, *Nature* **599**, 211 (2021).
- ⁵⁸ M. Bonifacio, F. Piazza, and T. Donner, *PRX Quantum* **5**, 040332 (2024).
- ⁵⁹ K. Baumann, C. Guerlin, F. Brennecke, and T. Esslinger, *Nature* **464**, 1301 (2010).
- ⁶⁰ J. Klinder, H. Keßler, M. Wolke, L. Mathey, and A. Hemmerich, *Proceedings of the National Academy of Sciences* **112**, 3290 (2015).
- ⁶¹ F. Mivehvar, H. Ritsch, and F. Piazza, *Phys. Rev. Lett.* **122**, 113603 (2019).
- ⁶² J. Klinder, H. Keßler, M. R. Bakhtiari, M. Thorwart, and A. Hemmerich, *Phys. Rev. Lett.* **115**, 230403 (2015).
- ⁶³ R. Landig, L. Hruby, N. Dogra, M. Landini, R. Mottl, T. Donner, and T. Esslinger, *Nature* **532**, 476 (2016).
- ⁶⁴ D. Lima, M. Grossklags, V. Zampronio, F. Cinti, and A. Mendoza-Coto, “Supersolid dipolar phases in planar geometry: effects of tilted polarization,” (2025), arXiv:2501.09641 [cond-mat.quant-gas].
- ⁶⁵ R. Lifshitz and D. M. Petrich, *Phys. Rev. Lett.* **79**, 1261 (1997).
- ⁶⁶ K. Jiang, J. Tong, and P. Zhang, *Communications in Computational Physics* **19**, 559 (2016).
- ⁶⁷ J. Yin, K. Jiang, A.-C. Shi, P. Zhang, and L. Zhang, *Proceedings of the National Academy of Sciences* **118**, e2106230118 (2021).
- ⁶⁸ S. Prestipino, A. Sergi, and E. Bruno, *Journal of Physics A: Mathematical and Theoretical* **52**, 015002 (2018).
- ⁶⁹ A. J. Leggett, *Phys. Rev. Lett.* **25**, 1543 (1970).
- ⁷⁰ A. J. Leggett, *Journal of Statistical Physics* **93**, 927 (1998).
- ⁷¹ P. B. Blakie, *Journal of Physics B: Atomic, Molecular and Optical Physics* **57**, 115301 (2024).
- ⁷² R. Gautier, H. Yao, and L. Sanchez-Palencia, *Phys. Rev. Lett.* **126**, 110401 (2021).
- ⁷³ L. P. Pitaevskii, *Sov. Phys. JETP* **13**, 451 (1961).
- ⁷⁴ E. P. Gross, *Journal of Mathematical Physics* **4**, 195 (1963).
- ⁷⁵ N. Masalaeva, H. Ritsch, and F. Mivehvar, *Phys. Rev. Lett.* **131**, 173401 (2023).
- ⁷⁶ F. Mivehvar, F. Piazza, T. Donner, and H. R. and, *Advances in Physics* **70**, 1 (2021), <https://doi.org/10.1080/00018732.2021.1969727>.
- ⁷⁷ F. Orsi, N. Sauerwein, R. P. Bhatt, J. Faltinath, E. Fedotova, N. Reiter, T. Cantat-Moltrecht, and J.-P. Brantut, *PRX Quantum* **5**, 040333 (2024).
- ⁷⁸ C. Mishra, S. Ostermann, F. Mivehvar, and B. P. Venkatesh, *Phys. Rev. A* **107**, 023312 (2023).
- ⁷⁹ M. Bonifacio, F. Piazza, and T. Donner, *PRX Quantum* **5**, 040332 (2024).
- ⁸⁰ G. R. Dennis, J. J. Hope, and M. T. Johnsson, *Computer Physics Communications* **184**, 201 (2013).